Journal of Sustainable Development of Energy, Water and Environment Systems

http://www.sdewes.org/jsdewes

Year 2024, Volume 12, Issue 1, 1110474

Original Research Article

Novel Design of Hybrid Single Slope Solar Distiller with Photovoltaic Powered Thermoelectric System

Mohammad Tariq Nasir*[1], Diaa Afaneh[2], Salah Abdallah[1] Hanan Saleet[1]

[1]Mechanical and industrial engineering department, Applied science private university, Amman, Jordan
e-mail: mo_nasir@asu.edu.jo*, salahabdalah@asu.edu.jo, h_saleet@asu.edu.jo

[2]Mechanical Engineering Department, King Fahd University of Petroleum and Minerals, Dhahran, Saudi Arabia
e-mail: diaa.afaneh@gmail.com

Cite as: Nasir, M., Afaneh, D., Abdallah, S., Saleet, H., Novel Design of Hybrid Single Slope Solar Distiller with Photovoltaic Powered Thermoelectric System, J.sustain. dev. energy water environ. syst., 12(1), 1110474, 2024, DOI: https://doi.org/10.13044/j.sdewes.d11.0474

ABSTRACT

This paper proposes a novel design for the Hybrid single slope Solar distiller with PV powered Thermoelectric, which is a sustainable and environmentally friendly alternative to provide purified water without burning fuel. The use of thermoelectric modules enhances the productivity of distilled water significantly. The design recovers part of the vapor latent heat and pumps it back to the saline water, which makes it more energy efficient compared to the traditional solar distiller. The experimental results show a remarkable 672% increase in productivity, highlighting the enormous benefits of the Hybrid single slope Solar distiller with PV powered Thermoelectric design compared to traditional distillers. Additionally, a mathematical model is formulated to simulate the proposed distiller behaviour, which shows an acceptable match with the experimental results.

KEYWORDS

Thermoelectric module, Solar energy, Distiller, Modelling and simulation.

INTRODUCTION

The distillation process is the most basic method for producing drinkable water from saline water. But this process is unsustainable since it uses energy produced by burning fossil fuel. Solar energy can be harvested and utilized to purify water. Thus, solar distiller is one sustainable and environment friendly alternative that recently has got the researcher attention. Distilled water has many applications in the industry such as: medical applications, laboratory experiments, cooling systems, pharmaceutical applications, cloth ironing, and battery manufacturing. The market size of the distilled water is growing rapidly [1].

Many directions to design distillers are followed in the literature, one environment friendly design is a distiller based on pure solar energy as an alternative green energy source [2]. The traditional solar distiller works by facing the saline water directly to the sun in the closed basin that is covered by an inclined glass sheet. The saline water will evaporate and then condensate forming water drops on the inner side of the glass cover; then these water drops slide and land in the drain.

The evolution and diversification of the traditional solar distiller's design is evident in various scholarly works. A primary focus has been on modifying the shape of the distiller to optimize solar energy absorption, thereby increasing the evaporation rate and distilled water

productivity. In [3], a novel pyramid chamber with a step-wise basin design is presented. Refinement of the pyramid shape by integrating reflectors, a cooling cycle, and wick cords to enhance performance is discussed in [4]. An empirical study in [5] evaluates the efficiency of pyramid-shaped solar stills. The concept of a hemispherical distiller, offering a distinct curvature to maximize solar interception, is elaborated upon in [6]. A comparison between the performance of both spherical and pyramid stills, each with a stepwise basin chamber design, is found in [7]. Progress made in inclined type solar still designs is highlighted in [8]. In [9], the effects of tray shapes in multi-stage solar stills when paired with a parabolic concentrating solar collector are investigated. Comparative analyses across these varied designs with traditional solar distillers indicate a significant enhancement in distilled water productivity.

In the second category, modifications incorporate heaters, specifically powered by Photovoltaic panels (PV), inside the saline-filled basin. This inclusion has been shown to promote evaporation and enhance productivity, as evidenced by [10] and [11]. The latter reference, [11], offers both experimental and numerical investigations into the utility of a semispherical solar still's stepwise basin, with and without the PV-powered heater, providing an insightful exploration into its practical applications. The third category emphasizes the use of special coatings on the basin to maximize solar energy absorption. Typically, the basin has been painted black due to its superior energy absorption properties compared to other colors. However, recent advancements, such as those discussed in [12], have explored the application of nano-technology-based coatings on the condensing surface, which further augments the productivity of solar stills. The fourth category introduces the concept of incorporating phase change material within the basin, as outlined in [10]. This material is unique in its ability to absorb solar energy throughout the day and release it during the night. The result is a solar distiller with extended operational hours, covering both day and nighttime, leading to increased productivity.

In the fifth category a sun tracking mechanism is added to allow the system to rotate following the sum movement; which increases the time of incident solar radiation exposure. This will increase the power generated; increasing evaporation and then productivity [13]. The sixth category includes adding a cooling device to the glass cover. Since the vapor drops are condensed on the inner surface of the glass cover, the cooling device will increase the condensation rate allowing more distilled water to be produced [14], [15].

In the seventh category, the last one, thermoelectric module (TEM) is added to the solar distiller in different ways [16]. Thermoelectric module is a semiconductor device that can force heat to flow from low temperature side to high temperature side while consuming electrical power.

TEM has two sides the hot and the cold side, the heat flux will be generated between the cold and the hot sides due to the Seebeck effect, in other words, TEM will pump heat from the cold side to the hot side [17], [18]. TEM is used in refrigerators, dehumidifier, power generation and other applications.

TEMs were used to enhance solar distillers' performance using four different methods.

In the first method, TEM is used to increase vapor condensation [19], [20]. Thus, the TEM cold side is facing the vapor to increase the condensation rate. The hot side of the TEM will be attached to a fan and a heat sink to increase the cooling. The second method is using TEM for increasing the evaporation process. In this case, the TEM hot side is attached to the solar distiller basin; so that TEM will heat the water inside the basin [21].

Both first and the second methods uses TEM either for cooling or heating. In both cases TEM must consume energy. But, the third method uses TEM for both cooling and heating. TEM is used for heating and energy recovery at the same time. TEM is used for cooling the vapor to increase the condensation and heating the saline water for increasing the evaporation. This method is more energy efficient since the TEM will collect the heat from the vapor and pump it back to the saline water to reuse it to generate vapor [22], [23]. The fourth method uses the TEM as an electrical power generator since TEM can work in a reverse direction to

generate electricity by applying heat flux on its hot and cold sides [24]. This method is not efficient since the TEM efficiency is less than 0.2 [25]. The main drawbacks in the previous systems are: piping complexity, using extra pumps for water recirculation, and using other energy consuming devices. These systems consume more energy resulting in a decrease in its efficiency [22].

In this work, a novel design of Hybrid Solar distiller with PV powered Thermoelectric module (HSPT) distiller is proposed. It is a single slope solar purifier (distiller) integrated with PV powered thermoelectric system. This design is inspired by the thermoelectric distiller produced in [26]. The usage of TEM as a secondary actuation element in solar distillers for increasing both evaporation and condensation is proposed. The new design uses PV panel power to run the TEMs, which harvest heat from condensation. Since the new design has no water pumps, fans, or any energy consuming devices, and it is predicted that it will improve the productivity.

SYSTEM DESCRIPTION

In this section, both the traditional single slope solar distiller and the novel hybrid solar distiller with PV powered Thermoelectric module (HSPT) distiller are described. Both solar distillers were fabricated in the workshops located in the Applied Science Private University.

Design specifications

The traditional distiller and HSPT distiller are both made of 1.5 mm thick galvanized steel. The saline water basin (tank) is covered with glass cover allowing the solar rays to heat and evaporate the water. This vapor will condensate at the inside side of the glass cover and slide to the collector. Both distillers have similar dimensions including the saline water basin (tank) dimensions and the glass cover dimensions; as shown in Figure 1. The glass cover is 2.0 mm thick and it has a slope angle of 28°. The water level for both tanks is 5.0 cm high. This water level is selected to cover the thermoelectric module since it is 4.0 cm × 4.0 cm. Both distiller basins were painted with black color for increasing solar radiation absorption.

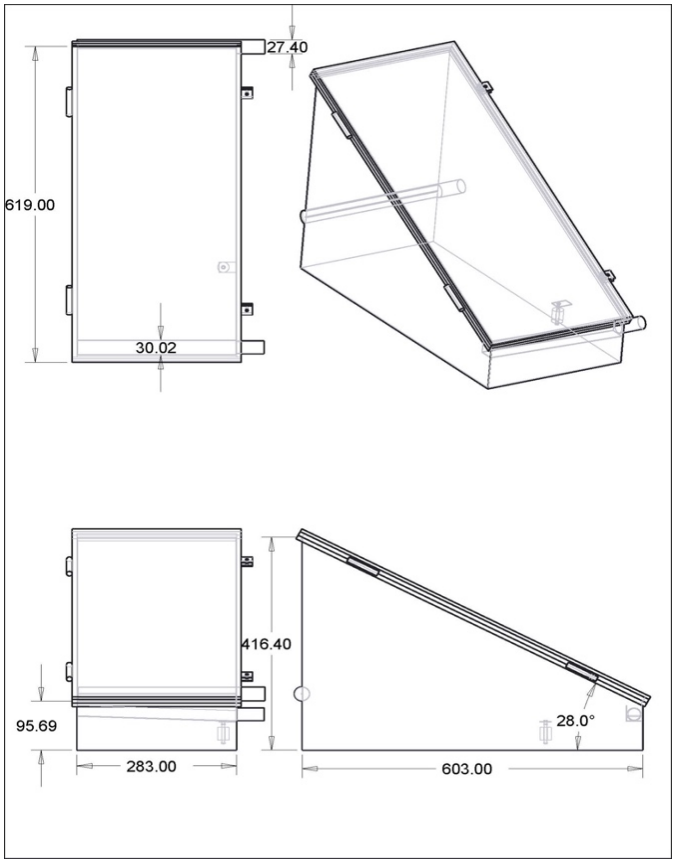

Figure 1. Traditional solar distiller dimension in (mm)

In addition, each distillers have stainless steel electrical level switch; these switches are normally closed type. There is a make-up tank connected with both basins by solenoid valve. The solenoid valves are wired to the electrical level switches in series, so that the electrical current will pass the solenoid once the water level decreases under the preset value of the level switch.

In the following, the novel design of HSPT is fully presented the HSPT distiller consists of two main tanks: the hot water tank (solar distiller basin that stores the saline water) and the cold-water tank (that collects the purified water). The dimensions of both tanks are shown in **Figure 2**. The thermoelectric modules are sandwiched between these two tanks, such that the hot side of the thermoelectric is attached to the solar basin and the TEM cold side is attached to the cold tank. On each side of the TEM, 3.0 mm thick aluminum plates are attached. In addition, aluminum plates are used instead of the galvanized steel for the inner side of the tanks. Because aluminum has higher thermal conductivity than the galvanized steel, the galvanized steel walls are replaced by aluminum plates. The cold tank has straight fins to increase condensation of water vapor. The hot tank was covered by wooden pieces insulating it from the surrounding weather conditions. However, the cold tank is not. It is painted in white color.

In the HSPT distiller, condensation takes place in two collectors. The first collector is indicated as number (1), see **Figure 2**. The vapor condenses at the inner side of the glass cover forming water drops which slides to this collector. The second collector is indicated as number (5), where condensation takes place at the inner side of the cold tank walls; especially at the aluminum plate that is attached to TEMs. **Figure 3** and **Figure 4** illustrate more HSPT distiller design and fabrication. **Figure 3** shows HSPT during manufacturing and **Figure 4** shows the hot tank, the cold tank and the glass cover for HSPT.

This novel design is considered an energy efficient system that increases distilled water productivity as will be proved by both the experimental work and simulation. In the HSPT distiller, the saline water in the hot tank is heated by two main sources: the solar radiation and the thermoelectric module. The Thermoelectric modules are sandwiched between the saline and the condensation tanks. The hot side of the thermoelectric module pumps the heat to increase saline water evaporation, and simultaneously it will increase condensation by recovering the latent heat from the vapor around the fins.

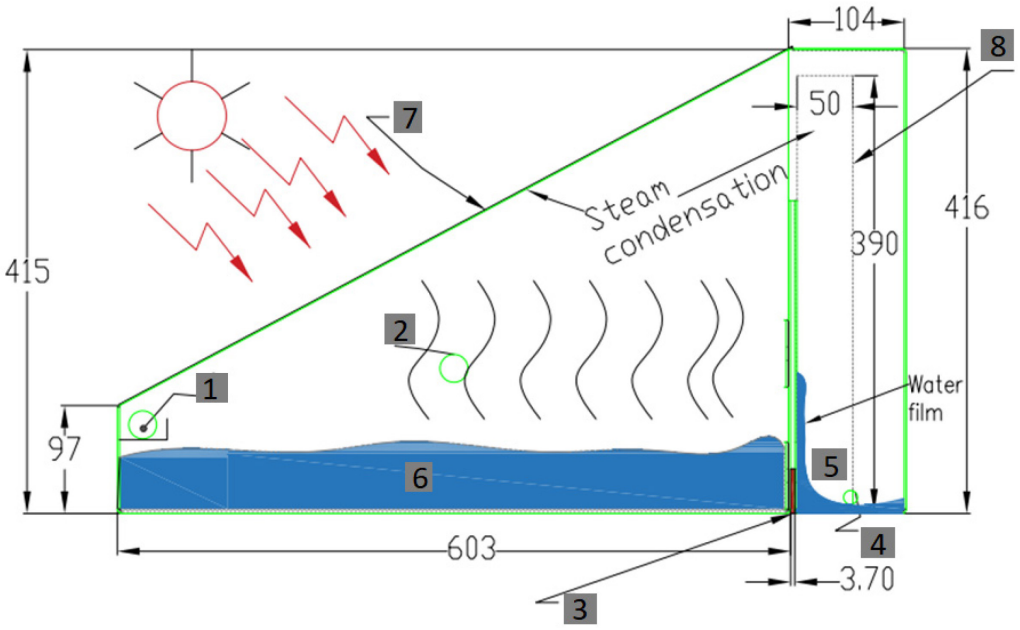

Figure 2. The HSPT dimension in mm: 1- purified water collector, 2- inlet water input, 3- thermoelectric module, 4- purified water output, 5- purified water tank, 6- saline water, 7- glass cover, 8- condensation fins

Figure 3. HSPT front view during manufacturing

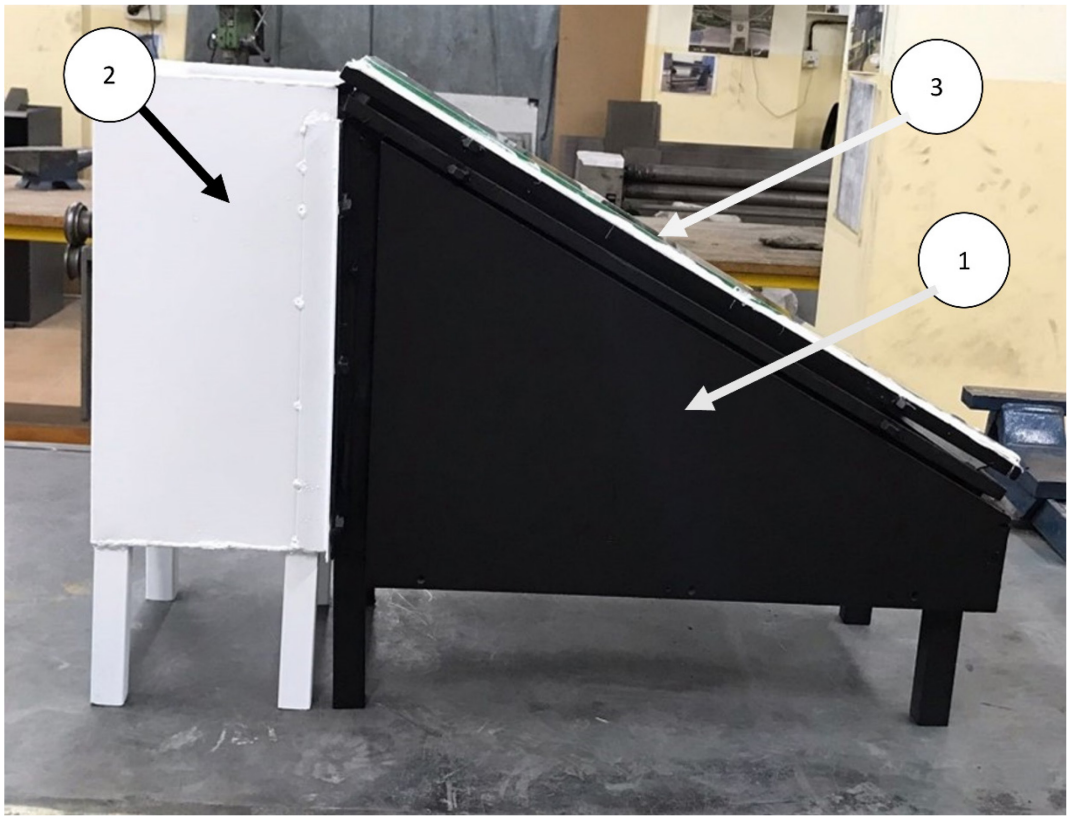

Figure 4. HSPT side view: 1- the hot tank, 2- the cold tank, 3- the glass cover

Mathematical modelling of the system:

The Thermoelectric module used in this paper is shown in eqs. (1), (2) and (3). Q_h and Q_c are the heat flow rate from the hot side (Q_h) and entering the TEM from the cold side (Q_c). α is the Seebeck coefficient and R is the electric resistance, k is the thermal conductance of the thermoelectric module, and $\Delta T = T_h - T_c$ is the temperature difference between the hot and cold sides of the TEM presented in eq. (4). These parameters are taken from the module datasheet with number TEC1-19908. Then, these parameters are validated experimentally by applying a simple least square fitting procedure for the collected reading of voltage, current and temperature; where the voltage loop presented in eq. (3) is used. The results are: $\alpha \cong 0.088$ V/K, $R \cong 2.38\ \Omega$ and $k \cong 0.8889$ W/K. The mathematical modelling will be explained more in this section.

$$Q_h = n\left[\alpha I T_h - k\Delta T + \frac{1}{2}I^2 R\right] \quad (1)$$

$$Q_c = n\left[\alpha I T_c - k\Delta T - \frac{1}{2}I^2 R\right] \quad (2)$$

$$V = n(IR + \alpha\Delta T) \quad (3)$$

$$\Delta T = T_h - T_c \quad (4)$$

In the following, HSPT mathematical model is derived. This model includes energy balance, mass balance and heat transfer equations. HSPT thermal model can be simplified into five main zones: 1) the glass cover model, 2) the water tank (basin) model, 3) the thermoelectric model, 4) the basin wall model, and 5) the cold-water film in the cold tank as shown in **Figure 5**.

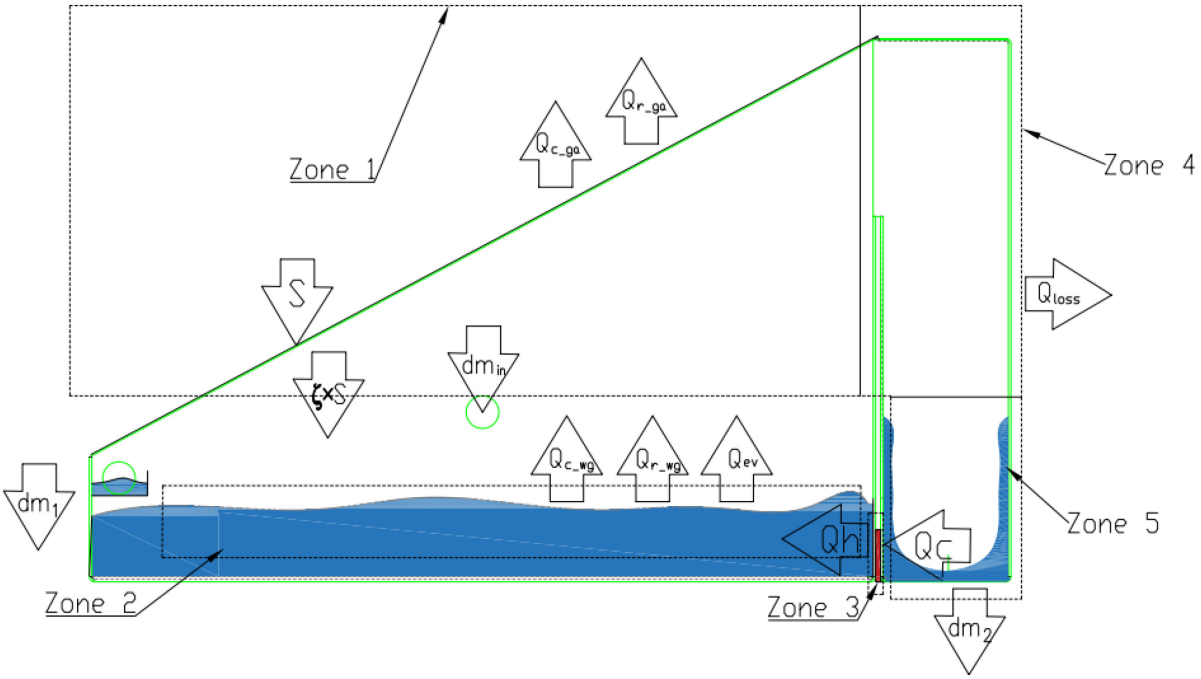

Figure 5. The thermal model diagram

At zone 1 (glass cover) eq. (5) presents Energy balance equation:

$$\dot{E}_{\text{in}_1} - \dot{E}_{\text{out}_1} = \frac{dT_\text{g}}{dt} m_\text{g} c_\text{g}, \tag{5}$$

where $\dot{E}_{\text{in}_1}$ is the energy entering the glass cover and it is found by eq. (6):

$$\dot{E}_{\text{in}_1} = \alpha_\text{g} S A_\text{g} + Q_{\text{c,wg}} + Q_{\text{r,wg}} + Q_{\text{ev,wg}} \tag{6}$$

and the solar energy absorbed by the glass is found in the term $\alpha_\text{g} S A_\text{g}$.

The convection heat transfer from the basin water to the glass cover $Q_{\text{c,wg}}$ is given by eq. (7):

$$Q_{\text{c,wg}} = h_{\text{c,wg}} A_\text{w} (T_w - T_\text{g}), \tag{7}$$

where $h_{\text{c,wg}}$ is calculated by eq. (8) found in [27]:

$$h_{\text{c,wg}} = 0.88 \left[T_\text{w} - T_\text{g} + \frac{(p_\text{w} - p_\text{g})(T_\text{w} + 273)}{268.9 \times 10^3 - p_\text{w}} \right]^{\frac{1}{3}}, \tag{8}$$

and the basin water saturated vapor pressure is p_w at basin water temperature T_w and pressure of the water saturated vapor p_g at glass temperature T_g is given by eqs. (9) and (10):

$$p_\text{w} = \exp\left(25.317 - \left(\frac{5144}{273 + T_\text{w}}\right)\right); \tag{9}$$

$$p_\text{g} = \exp\left(25.317 - \left(\frac{5144}{273 + T_\text{g}}\right)\right) \tag{10}$$

The radiation heat transfer rate from the basin water to the glass cover is found using eq. (11), presented by [28]:

$$Q_{\text{r,wg}} = h_{\text{r,wg}} A_\text{w} (T_\text{w} - T_\text{g}), \tag{11}$$

where the radiation heat transfer coefficient $h_{\text{r,wg}}$ is calculated using eqs. (12) and (13):

$$h_{\text{r,wg}} = \varepsilon_\text{e} \sigma \left[(T_\text{w} + 273)^2 + (T_\text{g} + 273)^2 \right] \left[(T_\text{w} + 273) + (T_\text{g} + 273) \right]; \tag{12}$$

$$\varepsilon_\text{e} = \frac{1}{\left(\frac{1}{\varepsilon_\text{g}}\right) + \left(\frac{1}{\varepsilon_\text{w}}\right) - 1} \tag{13}$$

The evaporation heat rate transfer from the water to the glass cover $Q_{\text{ev,wg}}$ is found by eq. (14); this equation was presented by [29]:

$$Q_{\text{ev,wg}} = h_{\text{ev,wg}} A_{\text{w}} (T_{\text{w}} - T_{\text{g}}), \tag{14}$$

where the evaporation heat transfer coefficient is found by eq. (15) and is given by [30]:

$$h_{\text{ev,wg}} = 16.273 \times 10^{-3} \times h_{\text{c,wg}} \times \left[\frac{p_{\text{w}} - p_{\text{g}}}{T_{\text{w}} - T_{\text{g}}}\right], \tag{15}$$

and the glass cover zone energy out is found in eq. (16):

$$\dot{E}_{\text{out}_1} = Q_{\text{c,ga}} + Q_{\text{r,ga}} + \frac{dm_1}{dt} h_{\text{gout}} \tag{16}$$

$\frac{dm_1}{dt}$ is the glass cover collected purified water production rate.

$Q_{\text{c,ga}}$ is the convective and radiation heat transfer rate from the glass cover to the surrounding ambient air and it is found by eq. (17), see reference [29]:

$$Q_{\text{c,ga}} = h_{\text{r,ga}} (T_{\text{g}} - T_{\text{a}}), \tag{17}$$

where the radiation heat coefficient $h_{\text{r,ga}}$ is found by eq. (18), see reference [31]:

$$h_{\text{r,ga}} = \varepsilon_{\text{e}} \sigma \left[\frac{(T_{\text{g}} + 273)^4 - (T_{\text{sky}} + 273)^4}{T_{\text{g}} - T_a}\right] \tag{18}$$

The sky temperature is found by eq. (18), see reference [32]:

$$T_{\text{sky}} = [0.0552 \times (T_{\text{a}} + 273)^{1.5} - 273] \tag{19}$$

At zone 2: Salty Water Energy balance, eq. (20):

$$\dot{E}_{\text{in}_2} - \dot{E}_{\text{out}_2} = \frac{dT_{\text{w}}}{dt} m_{\text{w}} c_{\text{p}}, \tag{20}$$

where the energy entering the zone is found by eq. (21):

$$\dot{E}_{\text{in}_2} = Q_{\text{Sw}} + Q_{\text{c,bw}} + \frac{dm_{\text{in}}}{dt} h_{\text{in}} + Q_{\text{h}}. \tag{21}$$

Q_{Sw} is the solar energy absorbed by the water, and found by eq. (22):

$$Q_{\text{Sw}} = \zeta \alpha_{\text{w}} S A_{\text{w}}, \tag{22}$$

where ζ is the glass transmittivity. $Q_{\text{c,bw}}$ is the rate of heat transfer from the basin wall to the water and found by eqs. (23) and (24):

$$Q_{\text{c,bw}} = h_{\text{c,bw}} A_{\text{b}} (T_{\text{b}} - T_{\text{w}}); \tag{23}$$

$$\dot{E}_{\text{out}_2} = Q_{\text{c,wg}} + Q_{\text{r,wg}} + Q_{\text{ev,wg}} + Q_{\text{ev,wwc}}, \tag{24}$$

where the $Q_{\text{ev,wwc}}$ is the evaporation heat transfer from the hot water inside the basin to the water film on inner side of the cold tank wall and the related heat transfer coefficient $h_{\text{ev,wwc}}$ is found by eq. (25),

$$Q_{\text{ev\_wwc}} = h_{\text{ev,wwc}} A_{\text{b}} (T_{\text{w}} - T_{\text{wc}}) \tag{25}$$

T_{wc} is the cold tank wall temperature, while the heat evaporation transfer coefficient between the water in the basin to the water film on the inner side of the cold tank is found by eq. (26):

$$h_{\text{ev,wwc}} = 16.273 \times 10^{-3} \times h_{\text{c,wwc}} \times \left[\frac{p_w - p_{\text{bc}}}{T_{\text{w}} - T_{\text{wc}}}\right]; \tag{26}$$

The convection heat coefficient between the water in the basin to the water film on the inner side of the cold tank is found by eq. (27):

$$h_{\text{c,wwc}} = 0.88 \left[T_{\text{w}} - T_{\text{wc}} + \frac{(p_{\text{w}} - p_{\text{b}})(T_{\text{w}} + 273)}{268.9 \times 10^3 - p_{\text{wc}}}\right]^{\frac{1}{3}}; \tag{27}$$

and the evaporation pressure near the water film inside the cold tank p_{wc} is found by eq. (28):

$$p_{\text{wc}} = \exp\left(25.317 - \left(\frac{5144}{273 + T_{\text{wc}}}\right)\right) \tag{28}$$

At zone 3: Thermoelectric Module energy balance is found by eq. (29):

$$\dot{E}_{\text{in}_3} - \dot{E}_{\text{out}_3} = 0 \tag{29}$$

The input energy is found by eq. (30):

$$\dot{E}_{\text{in}_3} = Q_{\text{c}} + P \tag{30}$$

The output energy is found by eq. (31):

$$\dot{E}_{\text{out}_3} = Q_{\text{h}} \tag{31}$$

where Q_c and Q_h are given in eqs. (1) and (2), while the thermoelectric input energy is found by eq. (32):

$$P = V \times I \tag{32}$$

At zone 4: Distiller Walls energy balance and the energy balance are found by eqs. (33), (34) and (35), where T_{b} is the basin temperature:

$$\dot{E}_{\text{in}_4} - \dot{E}_{\text{out}_4} = \frac{dT_{\text{b}}}{dt} m_{\text{b}} C_{\text{b}}; \tag{33}$$

$$\dot{E}_{\text{in}_4} = Q_{\text{Sb}}; \tag{34}$$

$$\dot{E}_{\text{out}_4} = Q_{\text{c,bw}} + U_{\text{b}} A_{\text{b}} (T_{\text{b}} - T_{\text{a}}) + U_{\text{b2}} A_{\text{b2}} (T_{\text{b}} - T_{\text{wc}}), \tag{35}$$

where A_{b} is the basin wall area, and the A_{b2} is the cold tank wall area. The basin outer wall is insulated by wooden cover to minimize the energy loss.

At zone 5: Cold Water film energy balance is found by eqs. (36), (37) and (38):

$$\dot{E}_{\text{in}_5} - \dot{E}_{\text{out}_5} = \frac{dT_{\text{wc}}}{dt} m_{\text{wc}} c_{\text{p}}; \tag{36}$$

$$\dot{E}_{\text{in}_5} = Q_{\text{ev,wwc}} + U_{\text{b2}} A_{\text{b2}} (T_{\text{wc}} - T_{\text{b}}), \tag{37}$$

where:

$$\dot{E}_{\text{out}_5} = Q_{\text{c}} + \frac{dm_2}{dt} h_{\text{out2}} \tag{38}$$

Note that the evaporation of the basin water is divided in three types; the evaporation from the basin water to the glass $Q_{\text{ev,wg}}$, the evaporation from the basin water to the basin wall $Q_{\text{ev,wb}}$ and the evaporation from the basin water to the cold water film inside the cold tank $Q_{\text{ev,wwc}}$. The total evaporation is found by eq. (39):

$$Q_{\text{ev}} = Q_{\text{ev,wg}} + Q_{\text{ev,wwc}} \tag{39}$$

Table 1. Parameters used in the simulation of the proposed solar distiller system

Parameter	Description	Value
c_p	Specific heat of water	4186
T_{s}	Sky temperature	$T_{\text{a}} - 6$;
V_{wind}	Wind speed	3 m/s
$h_{\text{c,gs}}$	Convection heat coefficient between the glass cover and the sky	$4.8 + 3.33 \times V_{\text{wind}}$
Ab	Basin area	(0.283×0.603) m^2

RESULTS

This section presents the results for the experimental work. Both the traditional and the HSPT distillers were tested under the same conditions. In addition, this section presents the simulation results which are based on the mathematical model. The simulation results and the experimental results proves the validation of the mathematical model.

Experimental results

The experiment was conducted during the summer of 2022, on the 16th of June. It took place at the Applied Science Private University, Renewable Energy Center in Amman, Jordan. In this experiment both the traditional solar distiller and the HSPT distiller were tested at the same conditions, as shown in **Figure 6**. In this section, the experimental results for both distillers are presented. These results are fully analyzed and discussed.

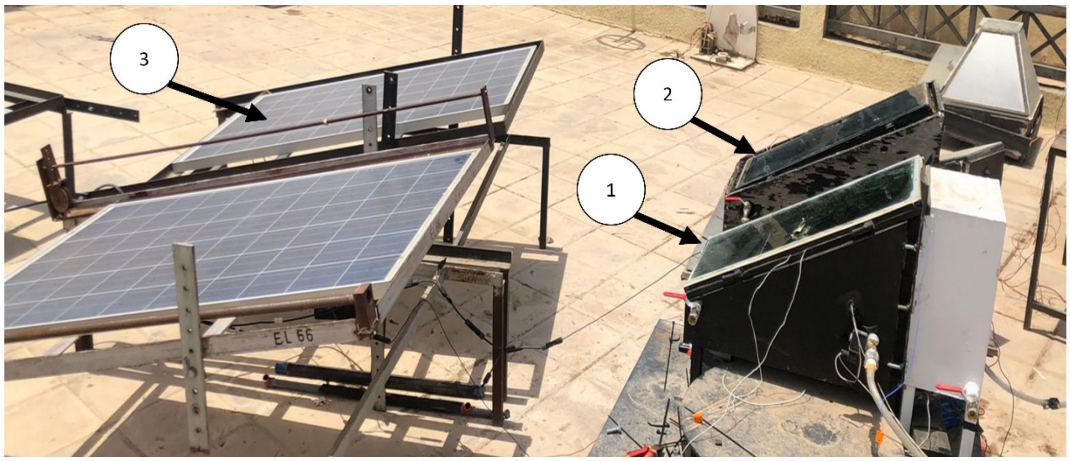

Figure 6. The experiment setup: 1- the HSPT, 2- the traditional solar distiller, and 3- the solar panel

Experimental results. **Table 2** shows the symbols used to describe the readings recorded for both distillers during the experiment. They are required to test the distillers' performance and to validate their capabilities.

Table 2: Symbols used to describe the readings recorded for both distillers

Symbol	Description
A	Current value (A)
Sol-Rad	Solar radiation (W/m^2)
T_a	Temperature of the surrounded environment
T_b	Temperature of the basin tank (hot tank) wall
T_c	TEM cold side temperature
T_h	TEM hot side temperature
T_g	Temperature of the glass cover
T_w	Temperature of the hot water in the basin
T_{wc}	Temperature of the water in the cold tank
TDS	Total dissolved solids (ppm)
V	Voltage value (V)

Table 3 shows the readings recorded for the HSPT distiller. As shown in the table, the photovoltaic solar panel starts producing current at 7:00 am. During the experiment both voltage and current are measured and used to calculate the power produced by the PV panel. The PV panel used has a maximum current is 8.0 A with approximately 30.0 V output without load. The maximum power measured in the experiment is reached at 11:00 am, when the current and voltage reach their maximum values. Since the solar panel converts sunlight to electricity, during this period of the day, the solar radiation reaches its maximum value; as shown in **Figure 7**.

Table 3. Readings recorded for the HSPT distiller on the 16th of June, 2022

Time	T_h (°C)	T_c (°C)	Tw (°C)	T_g (°C)	T_{wc} (°C)	T_b (°C)	*V* (volts)	*A* (Amp)	*TDS* (ppm)	Glass (mL/hour)	Tank (ml/hour)	Power (W)	T_a (°C)	Solar radiation W/m²
7:00	30	22	19	22	24	22	9.6	1.3	0	0	0	12.5	23.9	342
8:00	40.5	26	27	34	31	31	11	1.45	0	0	0	16	25.2	533
9:00	58	30	31	34	34	39	20.7	2.5	0	0	0	51.8	25.1	718
10:00	77	37	41	47	34	51	29.5	3.22	0	5	0	95	27.4	882
11:00	85	39	49	54	38	58	29.5	3.67	0	14	0	108.3	29.9	980
12:00	90	43	56	55	44	60	29.5	2.98	90	25	0	87.9	31.2	1000
13:00	94	53	63	57	47	62	28.8	2.85	85	35	55	82.1	32.3	952
14:00	95	50	63	58	48	64	28.6	2.8	73	55	80	80.1	32.8	897
15:00	96	52	65	58	50	67	29	2.84	69	55	88	82.4	32.9	765
16:00	93	49	63	57	48	65	28.8	2.87	67	58	92	82.7	33	590
17:00	84	45	60	52	45	60	25.2	2.56	39	37	62	64.5	32.2	376
18:00	54	40	52	45	39	50	7.7	0.85	32	38	73	6.5	30.6	159

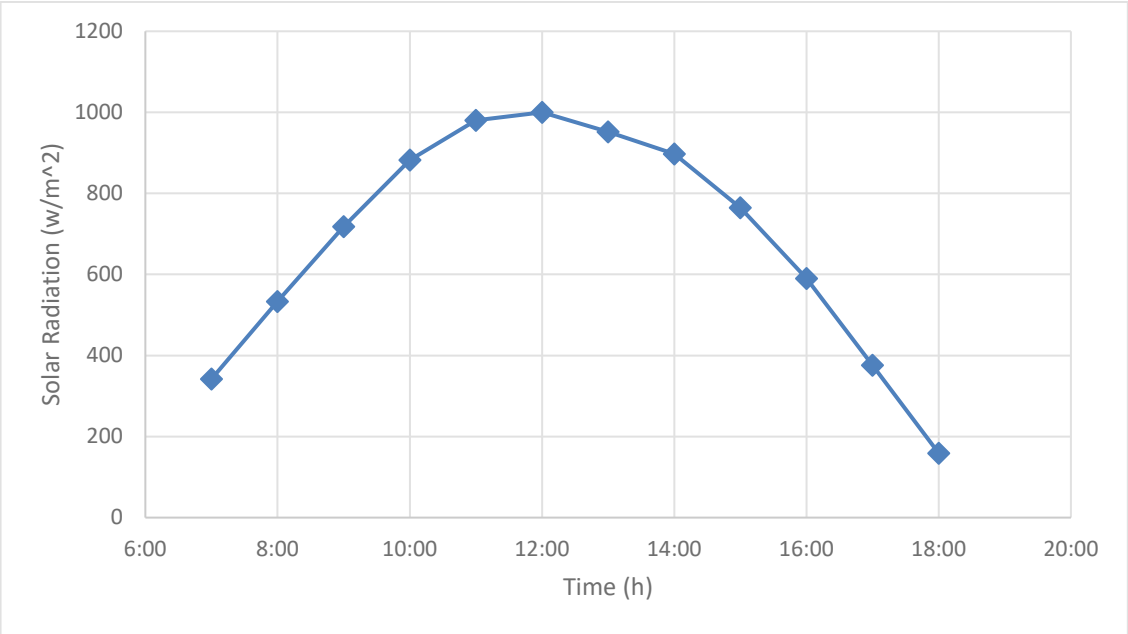

Figure 7. The Solar radiation on the 16th of June, 2022

The water temperature (T_w) at the beginning of the experiment was 19 °C at 7:00am; it reached its maximum value of 65 °C at 15:00. Figure 8 shows that the purified water is collected from two drains: the glass cover collector and the cold water tank. The purified water starts accumulating in the glass cover collector at 10:00; while it starts accumulating in the cold-water tank at 13:00. The delay in productivity of the cold water tank is due to the following three reasons. First, the humidity inside the distiller increases with the evaporation process. The evaporation process starts to accelerate after 12:00. Second, the vapor should travel longer distance to reach the cold side of the thermoelectric. This delayed the condensation of the vapor inside the cold water tank. Third, the cold water tank collector is design unproperly. Some water should be filled in this tank before it starts sliding through the valve; delaying the start of the readings.

The results shows that even though the surface area of TEM is much smaller than that of the glass, and even though the start point of distillation on glass was earlier than that of the TEM by 3 hours, the TEM productivity (ml/hour) is 1.4 times greater than that of the glass; as shown in **Figure 8**.

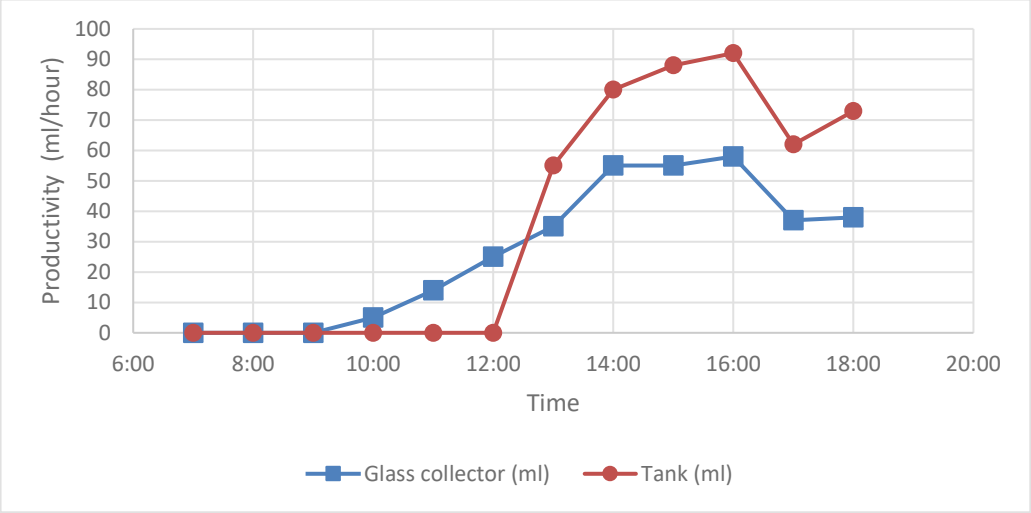

Figure 8. The purified water productivity using the HSPT showing both the glass collector and the cold tank productivity

Experimental results for traditional distiller compared to the Hybrid single slope Solar distiller with PV powered Thermoelectric. This section presents, analyzes, compare and discuss the experimental results for both distillers. **Table 4** shows the experimental results when using the traditional distiller. The novel design of the HSPT uses TEM as a secondary actuation element in HSPT distillers for increasing both evaporation and condensation enhances the distiller productivity. The experimental work involving both traditional distiller and the HSPT proves this statement The results are displayed in **Figure 9** which shows that the effect of the TEM as a source of heat starts approximately at 10:00. At 10: 00, both the glass cover temperature (T_g), see **Figure 9a**, and the basin tank (hot tank) wall temperature (T_b), see **Figure 9b**, of the HSPT distiller is higher than that of the traditional one. This is true, even though they are both in the same location; similar weather temperature and similar solar radiation. In addition, they have the same power source where the two PV panels attached to the two distillers have the same properties.

Table 4. Readings recorded for the traditional distiller on the 16th of June, 2022

Time	T_w (°C)	T_g (°C)	T_b (°C)	Productivity mL/hour	T_{atm} (°C)	Solar Radiation (w/m^2)
7:00	20	34	30	0	23.9	342
8:00	21	35	31	0	25.2	533
9:00	23	36	32	0	25.1	718
10:00	24	40	35	0	27.4	882
11:00	26	48	37	0	29.9	980
12:00	28	53	53	4	31.2	1000
13:00	44	58	54	3.5	32.3	952
14:00	46	56	62	14	32.8	897
15:00	46	55	57	15	32.9	765
16:00	52	50	53	19	33	590
17:00	52	41	41	23	32.2	376
18:00	48	41	43	21	30.6	159

(a)

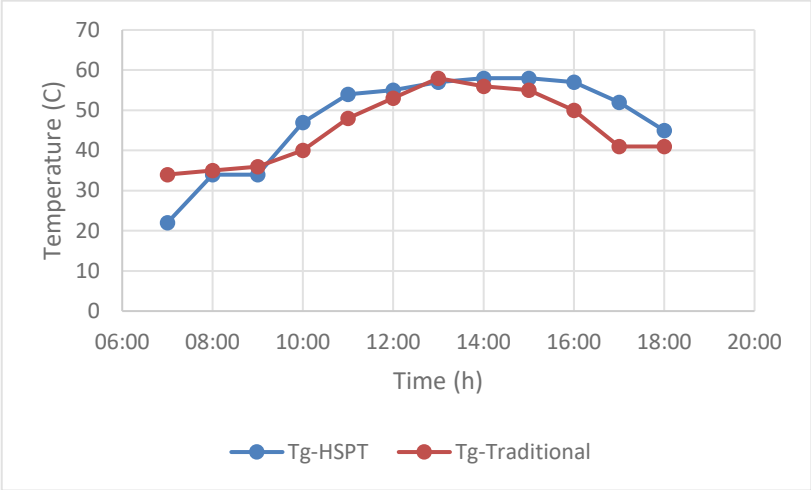

(b)

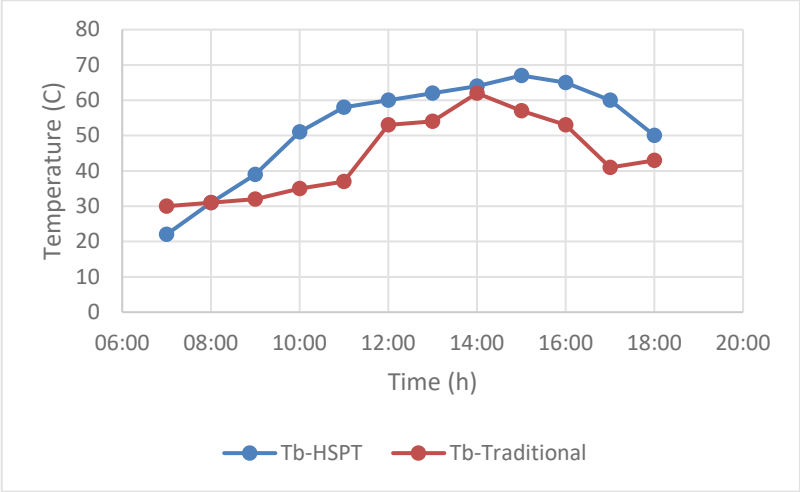

Figure 9. A comparison between the HSPT and the traditional distiller: a) temperature of the glass cover, b) temperature of the basin tank (hot tank) wall

In addition, comparing the water temperature in the hot tank for both distillers assure the effect of TEM as a heating source. The water temperature is very close to the wall temperature in the HSPT while it is different for the traditional one; as shown in **Figure 10**. Since the walls are made from metal, they heat up and then have high temperature compared to the water stored inside the hot tank. This is true in case that there is no energy source except the solar radiation; as in the case of the traditional distiller. **Figure 10a** shows this behavior for the traditional distiller. T_w and T_b are different, this is because the walls heat up faster and gain higher temperature compared to water. In addition, for points 16:00 to 18:00 on the *x*-axis, the water inside the traditional distiller keeps its energy for a longer time than the does the metal walls.

On the other hand, in case of HSPT, the difference between T_w and T_b is much smaller. This proves that the water is heated up by the energy harvested in the cold tank by the TEM, which is pumped back to the saline water basin for reuse. In addition, **Figure 10b** shows that, both basin wall and the water inside the basin have the same temperature for points 16:00 to 18:00 on the *x*-axis. This is again because of the heating effect of the TEM.

(a)

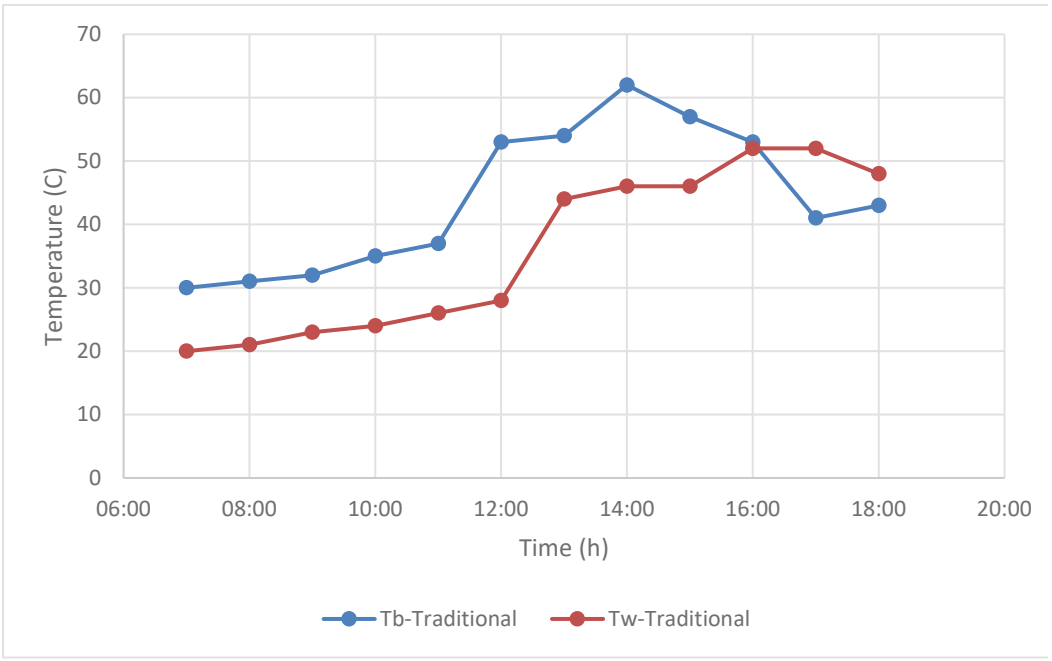

(b)

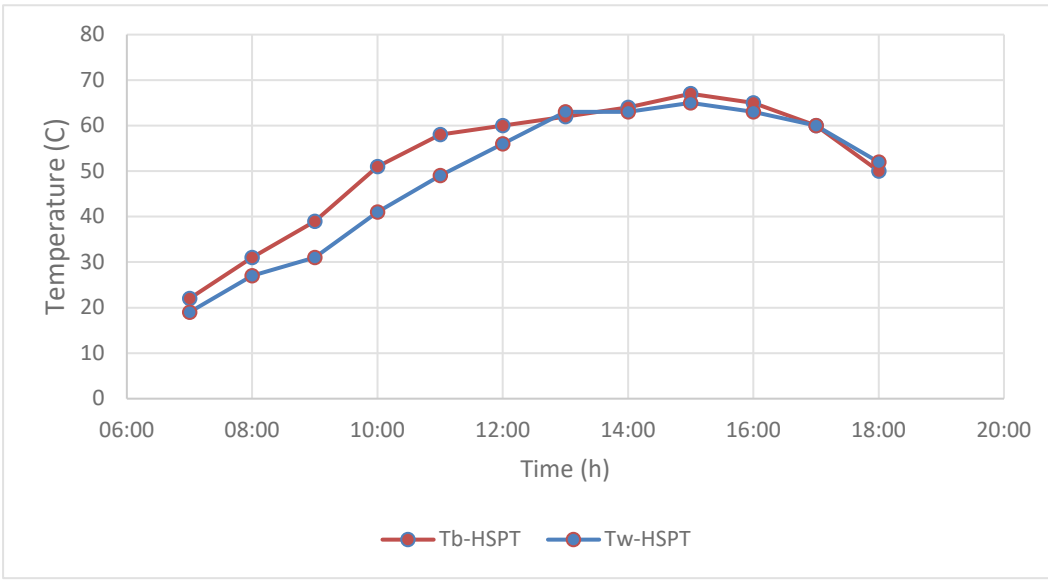

Figure 10. A comparison between T_b the wall temperature (a), and T_w the water temperature (b) for both HSPT and the traditional distiller

Figure 11 shows the increase in water temperature (T_w) for both distillers. For the traditional distiller, the water temperature is 20 °C at 7:00 and reach its maximum value of 52 °C at 16:00. For the HSPT distiller, the water temperature is 19 °C at 7:00 am and reach its maximum value of 65 °C at 15:00. The difference of 13 °C (65 °C – 52 °C) degrees between the maximum values of water temperature for both distillers highlights the contribution of the thermoelectric module in the heating process. This difference in water temperature directedly affects the productivity. Thus, the use of the TEM in the HSPT distiller hugely increases its productivity compared to the traditional one; as shown in **Figure 12**.

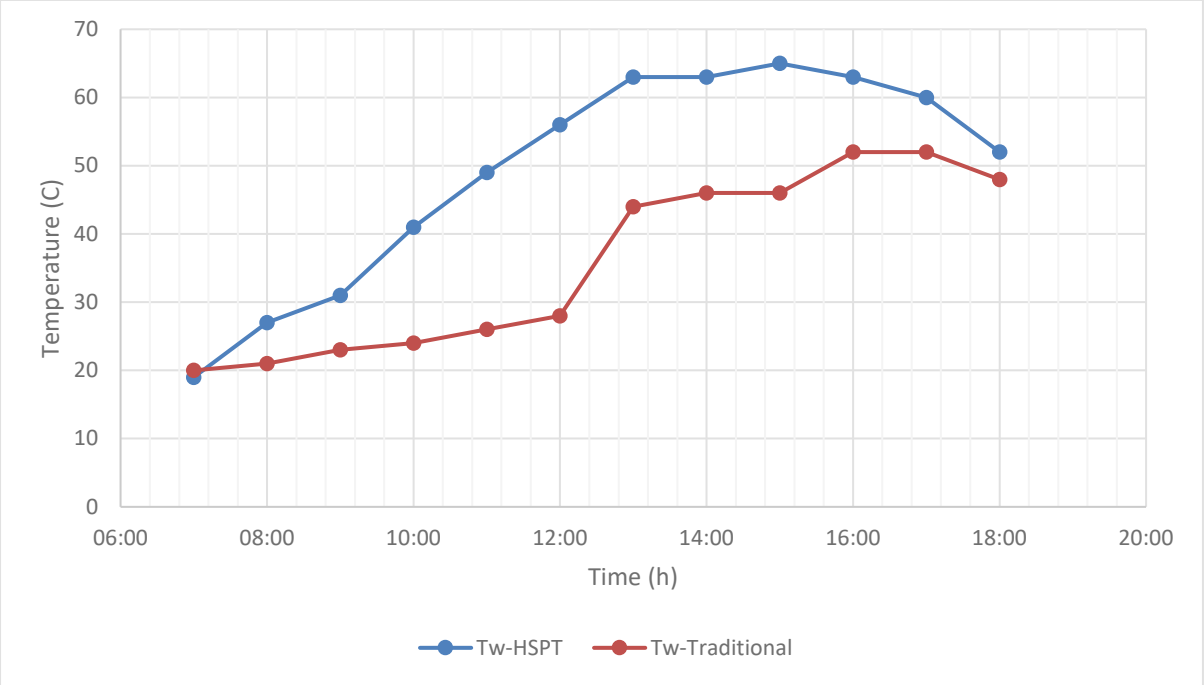

Figure 11. A comparison between the water temperature of HSPT distiller with the traditional solar distiller

In addition, **Figure 12** shows that the traditional distiller starts producing water at 12:00 compared to the HSPT distiller which starts producing purified water at 10:00. The max productivity of the traditional solar distiller is found 23 ml/hour and the max productivity of the HSPT solar distiller is 150 mL/hour; which emphases the huge increase in productivity as a result of utilizing the TEM. In addition, this increase in productivity per day can be calculated as follows: the total production per day for HSTP (772 mL/day) minus that for traditional distiller (99.5 mL/day) divided by (99.5 mL/day) equals 672%. This 672% increase in productivity is achieved by the following factors:

1) the thermoelectric module adds more heat in the case of HSPT distiller compared to the heat generated by the solar radiation alone in case of the traditional distiller.

2) the thermoelectric module absorbs heat from the vapor causing water to condensate on the cold side of the TEM modules.

3) the energy harvested in the cold tank is pumped back to the saline water basin for reuse it in evaporating process resulting in enhanced productivity.

4) the thermoelectric cold side temperature is less than glass cover temperature for both HSPT and the traditional solar distiller; this will increase the condensation in the cold tank compared to the glass cover in both distillers.

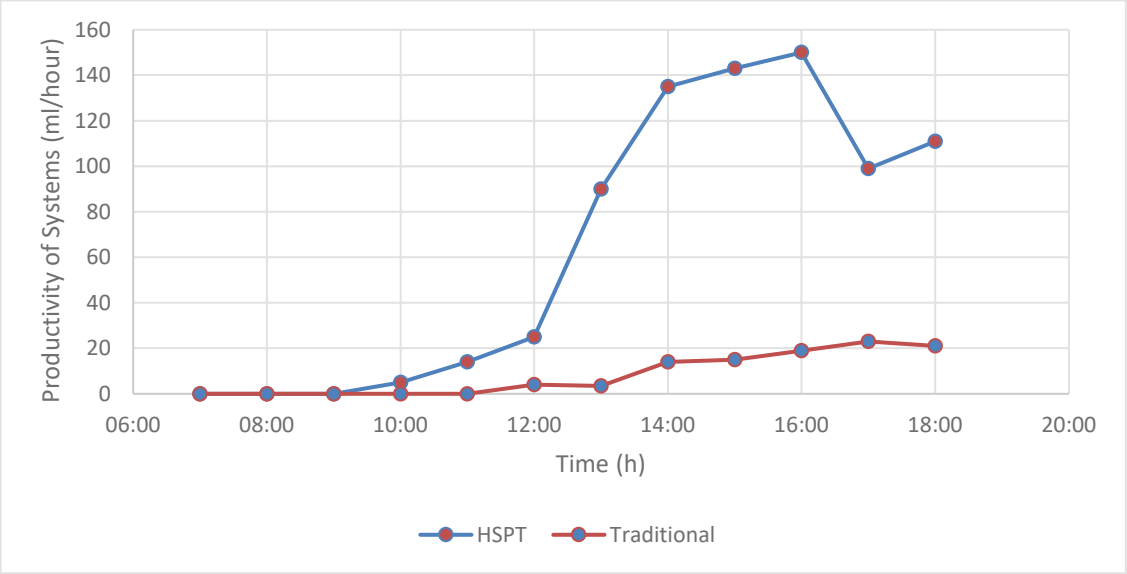

Figure 12. A comparison between the HSPT productivity with the traditional solar distiller productivity at the same conditions on the 16th of June, 2022

Increase the production of HSPT by 672% is considered promising compared to the increase in productivity addressed by previous design enhancements suggested by the journal papers published by the authors of this paper. These authors, in cooperation with others, has published a number of publications presenting the results of novel designs of the solar distiller. These novel designs are implemented and experimented in the same location as the novel design discussed in this paper. **Table 5** presents these publications and their contribution to the increase of productivity compared to the novel design presented in this paper.

In addition to the increase of productivity the efficiency of the HSPT distiller is 33% much more efficient compared to the traditional solar still that has 8% efficiency considering the solar power gained from PV and directly through the distiller class cover, and a night production for HSBT equals 300 ml, and for the traditional still equals 100 ml.

Comparison between simulation and experimental results

In this section the simulation model is validated by comparing the simulation results to the experimental results achieved in by the HSPT distiller. The simulation is based on the proposed mathematical model explained in section 1.2, and it is built using MATLAB Simulink software. The simulation model uses the parameters listed in **Table 1**. It consists of a set of differential equations which took 6 hours to be simulated and solved using MATLAB.

The simulation model shows an acceptable matching between experimental and simulation results as depicted in **Figure 13**. But there are a number of reasons why there are some mismatches. First, the variable heat losses in the distiller. Second, the cold-water tank collector is design unproperly. Some water should be filled in this tank before it starts sliding through the valve, delaying the start of the readings. other expected enhancement by considering the shading from still side walls.

Table 5. Publications and their contribution to the increase of productivity

Publication	Increase in productivity	New design	Compared to
Abdallah and Saleet, 2020 [3]	88.95%	A pyramid shape with three different faces and a step-wise chamber	Traditional solar distiller
Abdallah, *et al,* 2021 [33]	57.1%	Solar distiller has a spherical shape and a Step-wise chamber	A pyramid shape with three different faces and a step-wise chamber
Abdallah and Abu-Malouh,2021 [13]	242%	Inclined-type distiller with external mirror as a collecting element and one-axis sun-tracking mechanism	Traditional solar distiller
Aldarabseh and Abdallah, 2022 [11]	156.6%	A semispherical and chamber stepwise basin solar distiller, with and without photovoltaic (PV)-powered electrical heaters as another power source.	Traditional solar distiller
Aldarabseh and Abdallah, 2022 [34]	235.36 %	A semispherical solar distiller with a semicircular cross-sectional area and chamber stepwise basin with an automated single-axis sun-tracking with photovoltaic (PV)-powered electrical heaters	Traditional solar distiller
HSPT (This work)	672%	HSPT: utilizing thermoelectric module for heating and cooling	Traditional solar distiller

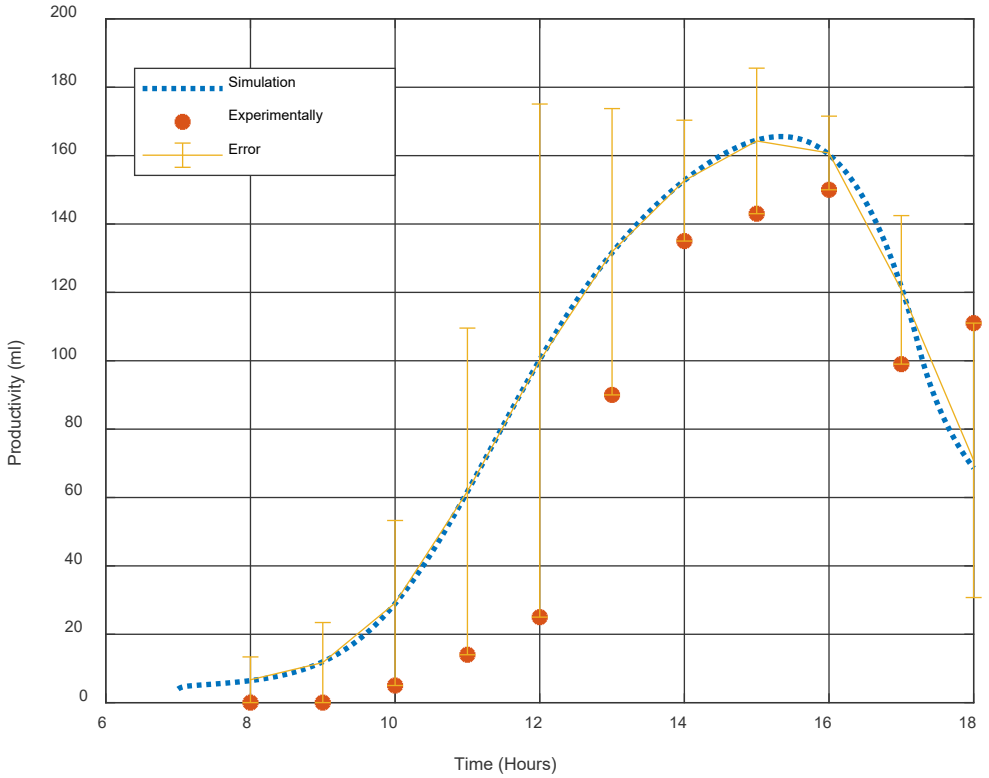

Figure 13. A comparison between the HSPT results with simulation results

CONCLUSION

Most traditional technologies for producing distilled water are unsustainable since they depend on burning fossil fuel. Finding new sustainable distillation methods is a need nowadays. In this paper, a novel design for the hybrid single slope solar distiller with PV powered thermoelectric (HSPT) was proposed, implemented, and tested. This distiller utilizes solar radiation and thermoelectric modules for heating the saline water. The thermoelectric modules provide extra important function, where it recovers part of vapor latent heat while condensing this vapor and pumping its heat back to the saline water. Experimental work was conducted in order to compare HSPT distiller performance to that of the traditional one. The results show 672% increase in productivity which emphases the enormous benefit of HSPT that utilizes the thermoelectric modules compared to the traditional distiller. A mathematical model is also formulated to simulate the HSPT distiller behaviour. The simulation of the mathematical model shows an acceptable matching with the experimental results. For the future work, the use of solar collectors or tracking systems can be utilized to enhance the system performance.

NOMENCLATURE

c_p	heat capacity of the water	[J/kgK]
$h_{c,bw}$	thermal convection coefficient between the water inside the basin and the basin walls	[W/m^{2}K]
$h_{c,gs}$	thermal convection coefficient between glass cover and the sky	[W/m^{2}K]
$h_{c,wg}$	thermal convection coefficient between the water inside the basin and the glass cover	[W/m^{2}K]

$h_{c,bw}$	thermal convection coefficient between the water inside the basin and the basin walls	[W/m^{2}K]
$h_{c,gs}$	thermal convection coefficient between glass cover and the sky	[W/m^{2}K]
$h_{c,wg}$	thermal convection coefficient between the water inside the basin and the glass cover	[W/m^{2}K]
$h_{c,wwc}$	thermal convection coefficient between the water inside the basin and the water film on the inner side of cold tank wall	[W/m^{2}K]
$h_{ev,wg}$	thermal evaporation coefficient between the water inside the basin and the glass cover	[W/m^{2}K]
$h_{ev,wwc}$	thermal evaporation coefficient between the water inside the basin and the water film on the inner side of cold tank wall	[W/m^{2}K]
h_{gout}	enthalpy of the exit water from the glass cover drain	[kJ/kg]
h_{in}	enthalpy of the inlet water at 25 °C	[kJ/kg]
$h_{r,ga}$	thermal radiation coefficient between the glass cover and the surrounding air	[W/m^{2}K]
$h_{r,wg}$	thermal radiation coefficient between the water inside the basin and the glass cover	[W/m^{2}K]
I	TEM inlet current	[A]
m_{hw}	total water mass in the hot tank	[kg]
m_1	mass of the purified water from the glass cover drain	[kg]
m_2	mass of the inlet water	[kg]
$\dot{m}_{cond}$	mass flow rate of the produced water (condensation)	[kg/s]
$\dot{m}_{in}$	mass flow rate of the inlet water	[kg/s]
n	number of TEM connected in parallel	[-]
P	electrical power consumed by the TEMD	[W]
Q_h	heat flux of the TEM hot side	[W]
Q_c	heat flux of the TEM cold side	[W]
$Q_{c,bw}$	convection heat transfer rate from the basin wall to the water inside the basin	[W]
$Q_{c,ga}$	convection heat transfer rate from the glass cover to the air surrounding	[W]
$Q_{c,wg}$	convection heat transfer rate from the hot water in the basin to the glass cover	[W]
$Q_{ev,wg}$	evaporation heat transfer rate from the hot water in the basin to the glass cover	[W]
$Q_{ev,wwc}$	evaporation heat transfer rate	[W]

	from the hot water in the basin to the water film on the cold tank walls	
$Q_{r,ga}$	radiation heat transfer rate from the glass cover to the air surrounding	[W]
$Q_{r,wg}$	radiation heat transfer rate from the hot water in the basin to the glass cover	[W]
Q_{sb}	solar energy rate absorbed by the basin walls	[W]
Q_{sw}	solar energy rate absorbed by the water	[W]
R	TEM electrical resistance	[Ω]
R_{out}	thermal resistance between the system and the environment	[J/kgK]
T_h	TEM hot side temperature	[K]
T_{atm}	temperature of the surrounded environment	[K]
T_b	temperature of the basin tank (hot tank) wall	[K]
T_{b2}	temperature of the cold tank wall	[K]
T_c	TEM cold side temperature	[K]
T_g	temperature of the glass cover	[K]
T_{sky}	temperature of the sky	[K]
T_w	temperature of the hot water in the basin	[K]
T_{wc}	temperature of the water in the cold tank	[K]
TDS	total dissolved solids	[ppm]
U	overall heat transfer coefficient	[W/m^{2}K]
V	voltage source value	[V]
W_{wind}	wind speed	[m/s]

Greek letters

α	Seebeck effect coefficient	[V/K]
ρ	water density	[kg/m^3]

ACKNOWLEDGEMENT

The authors are grateful to the Applied Science Private University, Amman, Jordan for the full financial support granted to this research project. The work is part of a funded project at Applied Science Private University with number DRGS-2021-2022-2.

REFERENCES:

1. DBRM, “Global Distilled Water Market - Industry Trends and Forecast to 2030," 2023. [Accessed: 28.09.2023] https://www.databridgemarketresearch.com/reports/global-distilled-water-market.
2. T. Rajaseenivasan, K. K. Murugavel, T. Elango, and R. S. Hansen, "A review of different methods to enhance the productivity of the multi-effect solar still," vol. 17, pp. 248-259, https://doi.org/10.1016/j.rser.2012.09.035.
3. S. Abdallah and H. Saleet, "Enhancing Productivity of Solar Still with Pyramid Chamber Step-Wise Basin Design," in Proceedings of International Conference of Aerospace and

Mechanical Engineering 2019: AeroMech 2019, 20-21 November 2019, Universiti Sains Malaysia, Malaysia, 2020, pp. 81-89, https://doi.org/10.1007/978-981-15-4756-0_8.
4. F. A. Essa, W. H. Alawee, S. A. Mohammed, A. S. Abdullah, and Z. M. Omara, "Enhancement of pyramid solar distiller performance using reflectors, cooling cycle, and dangled cords of wicks," vol. 506, p. 115019, https://doi.org/10.1016/j.desal.2021.115019.
5. Y. Taamneh and M. M. Taamneh, "Performance of pyramid-shaped solar still: Experimental study," vol. 291, pp. 65-68, https://doi.org/10.1016/j.desal.2012.01.026.
6. M. E. H. Attia, A. E. Kabeel, M. Abdelgaied, W. M. El-Maghlany, and A. Bellila, "Comparative study of hemispherical solar distillers iron-fins," vol. 292, p. 126071, https://doi.org/10.1016/j.jclepro.2021.126071.
7. S. Abdallah, M. Nasir, and D. Afaneh, "Performance evaluation of spherical and pyramid solar stills with chamber stepwise basin," vol. 218, pp. 119-125, https://doi.org/10.5004/dwt.2021.27009.
8. K. K. Murugavel, P. Anburaj, R. S. Hanson, and T. Elango, "Progresses in inclined type solar stills," vol. 20, pp. 364-377, https://doi.org/10.1016/j.rser.2012.10.047.
9. A. Abdessemed, C. Bougriou, D. Guerraiche, and R. Abachi, "Effects of tray shape of a multi-stage solar still coupled to a parabolic concentrating solar collector in Algeria," vol. 132, pp. 1134-1140, https://doi.org/10.1016/j.renene.2018.08.074.
10. M. T. Chaichan and H. A. Kazem, "Water solar distiller productivity enhancement using concentrating solar water heater and phase change material (PCM)," vol. 5, pp. 151-159, https://doi.org/10.1016/j.csite.2015.03.009.
11. S. M. Aldarabseh and S. Abdallah, "Experimental and Numerical Investigation of a Semispherical Solar Still, Chamber Stepwise Basin, With and Without a Photovoltaic-Powered Electrical Heater," vol. 144, no. 3, p. 31006, https://doi.org/10.1115/1.4053461.
12. P. Zanganeh, A. S. Goharrizi, S. Ayatollahi, and M. Feilizadeh, "Productivity enhancement of solar stills by nano-coating of condensing surface," vol. 454, pp. 1-9, https://doi.org/10.1016/j.desal.2018.12.007.
13. S. Abdallah and R. Abu-Malouh, "Design modifications of inclined-type single slope solar still with collecting element and sun-tracking mechanism," vol. 224, pp. 47-54, https://doi.org/10.5004/dwt.2021.27161.
14. O. M. Haddad, M. A. Al-Nimr, and A. Maqableh, "Enhanced solar still performance using a radiative cooling system," vol. 21, no. 3, pp. 459-469, https://doi.org/10.1016/S0960-1481(00)00079-3.
15. M. Abu-Arabi, Y. Zurigat, H. Al-Hinai, and S. Al-Hiddabi, "Modeling and performance analysis of a solar desalination unit with double-glass cover cooling," vol. 143, no. 2, pp. 173-182, https://doi.org/10.1016/S0011-9164(02)00238-2.
16. S. Shoeibi, H. Kargarsharifabad, M. Sadi, A. Arabkoohsar, and S. A. A. Mirjalily, "A review on using thermoelectric cooling, heating, and electricity generators in solar energy applications," vol. 52, p. 102105, https://doi.org/10.1016/j.seta.2022.102105.
17. D. Zhao and G. Tan, "A review of thermoelectric cooling: materials, modeling and applications," vol. 66, no. 1, pp. 15-24, https://doi.org/10.1016/j.applthermaleng.2014.01.074.
18. M. Elgendi, A. E. Kabeel, and F. A. Essa, "Improving the solar still productivity using thermoelectric materials: A review," Alexandria Engineering Journal, 2022, https://doi.org/10.1016/j.aej.2022.10.011.
19. N. T. Alwan et al., "Enhancement of the Evaporation and Condensation Processes of a Solar Still with an Ultrasound Cotton Tent and a Thermoelectric Cooling Chamber," vol. 11, no. 2, p. 284, https://doi.org/10.3390/electronics11020284.
20. M. A. Al-Nimr, W. A. Al-Ammari, and A. Alkhalidi, "A novel hybrid photovoltaics/thermoelectric cooler distillation system," vol. 43, no. 2, pp. 791-805, https://doi.org/10.1002/er.4309.

21. N. Rahbar, A. Gharaiian, and S. Rashidi, "Exergy and economic analysis for a double slope solar still equipped by thermoelectric heating modules-an experimental investigation," vol. 420, pp. 106-113, https://doi.org/10.1016/j.desal.2017.07.005.
22. S. Shoeibi, N. Rahbar, A. A. Esfahlani, and H. Kargarsharifabad, "Improving the thermoelectric solar still performance by using nanofluids-Experimental study, thermodynamic modeling and energy matrices analysis," vol. 47, p. 101339, https://doi.org/10.1016/j.seta.2021.101339.
23. S. M. Parsa, A. Yazdani, D. Javadi, M. Afrand, N. Karimi, and H. M. Ali, "Selecting efficient side of thermoelectric in pyramid-shape solar desalination units incorporated phase change material (PCM), nanoparticle, turbulator with battery storage powered by photovoltaic," vol. 51, p. 104448, https://doi.org/10.1016/j.est.2022.104448.
24. M. A. Al-Nimr and K. S. Qananba, "A solar hybrid thermoelectric generator and distillation system," vol. 15, no. 8, pp. 473-488, https://doi.org/10.1080/15435075.2018.1479266.
25. G. J. Snyder and T. S. Ursell, "Thermoelectric efficiency and compatibility," vol. 91, no. 14, p. 148301, https://doi.org/10.1103/PhysRevLett.91.148301.
26. M. T. Nasir, D. Afaneh, and S. Abdallah, "High productivity thermoelectric based distiller," vol. 206, pp. 125-132, https://doi.org/10.5004/dwt.2020.26295.
27. R. V Dunkle, "Solar water distillation: the roof type still and a multiple effect diffusion still," in Proc. International Heat Transfer Conference, University of Colorado, USA, 1961, vol. 5, p. 895.
28. T. L. Bergman, T. L. Bergman, F. P. Incropera, D. P. Dewitt, and A. S. Lavine, Fundamentals of heat and mass transfer. John Wiley & Sons.
29. Y. H. Zurigat and M. K. Abu-Arabi, "Modelling and performance analysis of a regenerative solar desalination unit," vol. 24, no. 7, pp. 1061-1072, https://doi.org/10.1016/j.applthermaleng.2003.11.010.
30. S. Kumar and G. N. Tiwari, "Estimation of convective mass transfer in solar distillation systems," vol. 57, no. 6, pp. 459-464, https://doi.org/10.1016/S0038-092X(96)00122-3.
31. O. O. Badran and M. M. Abu-Khader, "Evaluating thermal performance of a single slope solar still," vol. 43, no. 10, pp. 985-995, https://doi.org/10.1007/s00231-006-0180-0.
32. N. Akhtar and S. C. Mullick, "Computation of glass-cover temperatures and top heat loss coefficient of flat-plate solar collectors with double glazing," vol. 32, no. 7, pp. 1067-1074, https://doi.org/10.1016/j.energy.2006.07.007.
33. S. Abdallah, M. Nasir, and D. Afaneh, "Performance evaluation of spherical and pyramid solar stills with chamber stepwise basin," Desalination Water Treat, vol. 218, 2021, https://doi.org/10.5004/dwt.2021.27009.
34. S. M. Aldarabseh and S. Abdallah, "Stepped Semispherical Solar Still With PV Powered Electrical Heaters and an Automated Single-Axis Sun Tracker System," vol. 29, no. 8, https://doi.org/10.1615/JEnhHeatTransf.2022041845.

Paper submitted: 28.05.2023
Paper revised: 28.09.2023
Paper accepted: 03.10.2023